Microsc. Microanal. 15, 154–165, 2009
doi:10.1017/S1431927609090230

Microscopy AND Microanalysis

Ultrastructure of the Epithelial Cells Associated with Tooth Biomineralization in the Chiton *Acanthopleura hirtosa*

Jeremy A. Shaw,[1,*] David J. Macey,[2] Lesley R. Brooker,[3] Edward J. Stockdale,[1] Martin Saunders,[1] and Peta L. Clode[1]

[1]*Centre for Microscopy, Characterisation and Analysis, The University of Western Australia, Crawley, WA 6009, Australia*
[2]*School of Biological Sciences & Biotechnology, Murdoch University, Murdoch, WA 6150, Australia*
[3]*Faculty of Science, Health and Education, University of the Sunshine Coast, Maroochydore DC, QLD 4558, Australia*

Abstract: The cusp epithelium is a specialized branch of the superior epithelium that surrounds the developing teeth of chitons and is responsible for delivering the elements required for the formation of biominerals within the major lateral teeth. These biominerals are deposited within specific regions of the tooth in sequence, making it possible to conduct a row by row examination of cell development in the cusp epithelium as the teeth progress from the unmineralized to the mineralized state. Cusp epithelium from the chiton *Acanthopleura hirtosa* was prepared using conventional chemical and microwave assisted tissue processing, for observation by light microscopy, conventional transmission electron microscopy (TEM) and energy filtered TEM. The onset of iron mineralization within the teeth, initiated at row 13, is associated with a number of dramatic changes in the ultrastructure of the apical cusp cell epithelium. Specifically, the presence of ferritin containing siderosomes, the position and number of mitochondria, and the structure of the cell microvilli are each linked to aspects of the mineralization process. These changes in tissue development are discussed in context with their influence over the physiological conditions within both the cells and extracellular compartment of the tooth at the onset of iron mineralization.

Key words: TEM, EFTEM, EELS, microwave, iron, ferritin, organic matrix, magnetite

Introduction

Microscopy is commonly applied to the study of biomineralized tissues such as teeth, shell, or bone. Consequently, advances in the field of biomineralization have often followed new developments in microscopy-based techniques. This is in large part due to the inherent structural nature of biomineralized tissues, which are often assembled in a hierarchical manner that can be characterized at various spatial scales (Weiner, 2008). Many advances have been made in methods of tissue processing, such as microwave-assisted or cryogenic methods of sample preparation (McDonald et al., 2007; Webster, 2007). In addition, analytical techniques, such as energy-filtered transmission electron microscopy (EFTEM), which has normally been applied to samples in the materials sciences, is now more commonly being used to approach biological questions (Leapman, 2004; Leapman & Aronova, 2007). These techniques provide the opportunity to reexamine and extend our understanding of biomineralized tissues.

The formation of biomineralized structures normally occurs under strict biological control, where the organism mediates the solution chemistry within the confines of an extracellular organic matrix scaffold, acting as a template for mineral formation (Mann, 2001). Much of the fundamental understanding of organic matrix mediated biomineralization has resulted from the study of tooth mineralization in a relatively obscure class of marine mollusks, the Polyplacophora, or chitons (Fig. 1A) (Weiner & Addadi, 2002). Chitons exhibit an extraordinary and elegant level of control over tooth mineralization and have inspired modern materials scientists in search of novel technologies modeled on the biomimetic principles behind tooth formation. Furthermore, chitons play a key role in the ecology of intertidal habitats, where they have been shown to strongly influence algal community structure (Steneck & Watling, 1982; Scheibling, 1994) and contribute significantly in coastal bioerosion processes (Barbosa et al., 2008).

As is the case with the feeding apparatus of most mollusks, chitons possess a ribbon of repeating tooth rows

Received October 9, 2008; accepted January 14, 2009
*Corresponding author. E-mail: jeremy.shaw@uwa.edu.au

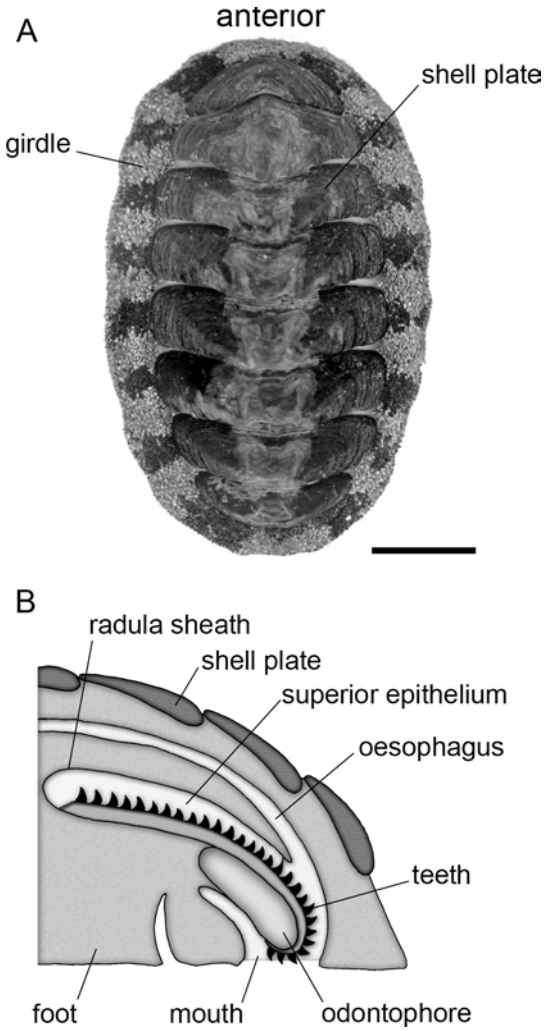

Figure 1. Characteristic body plan of a chiton. **A:** Dorsal surface of the chiton *A. hirtosa*, exhibiting eight shell plates mounted in a fleshy girdle; as is typical for all chitons. Scale bar = 1 cm. **B:** Diagrammatic representation of the feeding apparatus at the anterior end of the animal, depicting the general position of the radula and associated tissues.

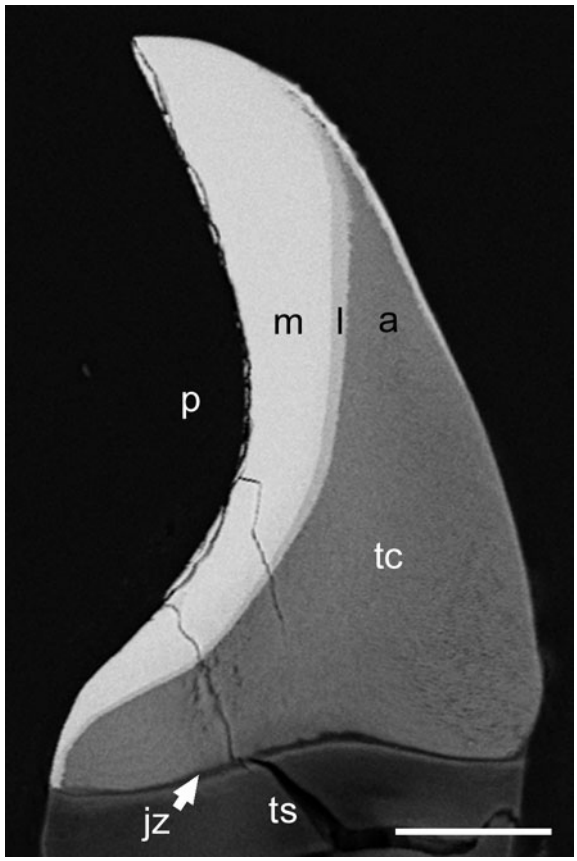

Figure 2. Backscattered scanning electron micrograph of a longitudinal section through a major lateral tooth from *A. hirtosa*, highlighting the overall internal structure of a mature tooth including the tooth base or stylus (ts), junction zone (jz), and tooth core (tc). In addition, the cusp is further divided into distinct mineral regions, which include magnetite (m), lepidocrocite (l), and apatite (a); p = posterior surface. Scale bar = 50 μm.

termed the radula (Fig. 1B), which is formed continuously to replace those lost as a result of feeding (Runham, 1963). However, unlike other mollusks, chitons utilize the iron oxide magnetite, together with a variety of other biominerals, to significantly harden their major lateral teeth. This reinforcement allows these mollusks to feed on algae living on, and within, the hard rock of their intertidal habitats (Lowenstam, 1962). Remarkably, each mineral phase forms in a stepwise fashion within architecturally discrete regions of each tooth cusp (Fig. 2) (Macey et al., 1996), with the whole process resembling a production line.

The elements required for mineralizing the teeth are primarily delivered by the cusp cell epithelium surrounding the teeth (Nesson & Lowenstam, 1985; Kim et al., 1989). Microscope observations of this epithelial tissue are difficult due to the progressive deposition of hard biominerals into the tooth cusps, which make thin sectioning highly problematic. For this reason, to date, much of the focus on tooth development has been directed at the onset of iron mineralization, where iron is first deposited within the tooth cusps. Two main studies describe the ultrastructure of chiton epithelial tissue. The first (Nesson & Lowenstam, 1985) details the ultrastructure of these cells in context with the iron-containing granules and microvilli that surround the teeth. The second (Kim et al., 1989) describes the ultrastructure of the epithelium in three tooth rows, including one row immediately prior to, one at, and one following, the onset of iron mineralization. However, our understanding of what happens to the structure of cells in tissue surrounding the teeth prior to, and following, the onset of mineralization remains limited. Recently, we demonstrated that the preservation of chiton superior epithelial tissue can be vastly improved relative to conventional bench top process-

Table 1. Acquisition Parameters for Iron, Nitrogen, and Oxygen EFTEM Mapping of Granules within the Cusp Epithelium of the Chiton *A. hirtosa*.

Element	Edge	Pre-Edge 1 (eV)	Pre-Edge 2 (eV)	Post-Edge (eV)	Slit Width (μm)	Acquisition Time (s)
Fe	$M_{2,3}$	45	50	59	5	15
N	K	346	376	416	30	120
O	K	484	514	547	30	120

ing, using microwave or cryogenic methods (Shaw et al., 2008*a*).

Accordingly, a detailed study of cell development within the apical cusp epithelium of the chiton *Acanthopleura hirtosa* has been undertaken using a combination of conventional and microwave-assisted tissue preservation, together with various light and electron microscopic techniques. A comprehensive investigation of the cells surrounding nine major lateral tooth rows is presented, including three rows prior to, and five rows following, the onset of mineralization at tooth row 13. Together, these new techniques provide the opportunity to reexamine the structure and composition of chiton epithelial tissue, with the aim of providing a significantly improved description of the cellular events that take place at the onset of mineralization.

Materials and Methods

Fresh specimens of the chiton *A. hirtosa* (Blainville, 1825, cited in Shaw et al., 2002) were collected and dissected as described previously (Shaw et al., 2008*a*). Briefly, radulae were excised and fixed in 2.5% glutaraldehyde, buffered in 0.1 M phosphate at pH 7.2 (osmotic pressure adjusted to 900 $mmol \cdot kg^{-1}$ using sucrose). Radulae were then fixed, dehydrated, and infiltrated in epoxy resin using either conventional chemical fixation ($n = 8$) or microwave-assisted chemical fixation ($n = 6$) (Pelco, Biowave). Figures are labeled with either *CF* or *MF* to denote either conventional or microwave fixation, respectively.

For light microscopy, 1-μm-thick sagittal sections through the major lateral teeth were cut in longitudinal orientation along the radula. Sections were mounted on glass slides and stained with aqueous 1% Methylene Blue and 1% Azur II (20 s) prior to being imaged on an optical microscope (Olympus BX51) fitted with a digital camera (Olympus DP70).

For conventional TEM, ~100-nm-thick sections were cut using a diamond knife (Diatome^{TM}) and mounted on either formvar-filmed or nonfilmed copper grids. Sections were observed either unstained at 120 kV in a TEM (JEOL, 2100), fitted with a digital camera (Gatan, Orius), or double stained with uranyl nitrate (single crystal in one drop of 50% methanol) (10 min) and Sato's lead citrate (10 min) (Hanaichi et al., 1986), and imaged at 80 kV in a TEM (JEOL, 2000) using plate film.

For EFTEM imaging and electron energy loss spectroscopy (EELS), unstained sections were mounted on uncoated or carbon coated copper grids and analyzed at 200 kV in a TEM (JEOL, 2100), fitted with a Gatan Imaging Filter (GIF, Tridiem). The EFTEM elemental maps were acquired using the conventional three-window method (see Brydson, 2001). The acquisition parameters used for iron, nitrogen, and oxygen mapping are outlined in Table 1. Thin sections were used to minimize the effects of plural inelastic scattering, all sections were cut to a thickness of ~80 nm, corresponding to a t/λ value of <0.5. To obtain suitable signal-to-noise levels, 4× binning was used.

Due to the extreme hardness of the mineralized teeth, thin sections cannot be obtained beyond tooth row 18. As such, data are presented from rows 10 to 18, which covers four tooth rows either side of the orange tooth, which has been described as the row following the onset of iron mineralization in *A. hirtosa* (Shaw et al., 2008*b*).

Results

The quality of superior epithelial tissue preservation observed between conventional bench top and microwave processed samples was consistent with that described previously by Shaw et al. (2008*a*). While the gross morphology and arrangement of organelles within the apical region of the superior epithelium was the same for tissue prepared using either method, far better preservation of fine structure was observed in tissue fixed using the microwave-assisted protocol.

Two major groups of columnar epithelium were identified in *A. hirtosa* radula tissue stained with Methylene Blue and Azur II. The first were the epithelial cells associated with the major lateral tooth cusps and thus involved in iron mineralization. The second, which for reasons unknown stained less intensely than the first, were those attached to the major lateral tooth bases and the remaining minor teeth (Fig. 3A). Only the epithelium involved in the developing major lateral tooth cusps (cusp cells) are considered here. Individual cusp cells extend from the lumen of the dorsal

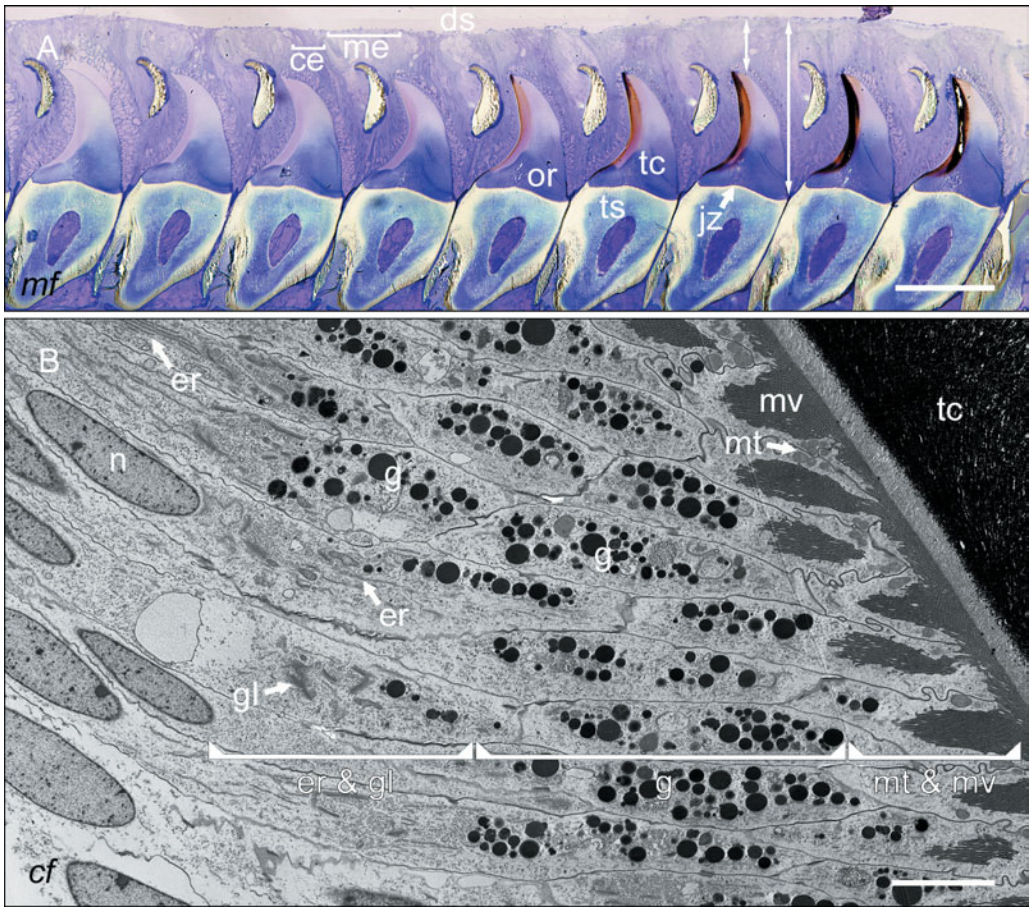

Figure 3. Superior epithelial tissue surrounding the tooth cusps (tc) and tooth styli (ts) of the chiton *A. hirtosa*. **A:** Light micrograph of major lateral tooth rows 10 to 18 in longitudinal section highlighting the respective light and dark staining minor (me) and cusp epithelium (ce) bordering the dorsal sinus (ds), the latter of which varies in length depending on where it attaches to the tooth cusp (short and long double arrows). Also note the position of the junction zone (jz) at the base of the cusp and the orange tooth (or) at row 14. **B:** TEM micrograph showing the typical structure of the cusp epithelium and the arrangement of organelles within the apical region of the cells at tooth row 17. Three main regions can be defined within the apical epithelium between the nuclei (n) and tooth cusp. These include the endoplasmic reticulum/Golgi (er and gl) region, the granule (g) region, and the mitochondria/microvilli (mt and mv) region. Scale bars = (**A**) 200 μm, (**B**) 5 μm.

sinus to make direct contact with either the anterior and posterior surface of each tooth and range in length from ~105 μm, where the cells attach to the cusp tip, to ~340 μm, where they extend to the base of the cusp above the junction zone (Fig. 3A). Regardless of length and surface contacted, each cell is approximately 4 μm in diameter and contains organelles that are typical of epithelia bordering extracellular compartments (Fig. 3B). A single prominent nucleus is located toward the apical half of each cell, 40–50 μm from the cusp surface (Fig. 3B). The area between the nucleus and apical pole of each cell is further organized into three distinct regions (Fig. 3B). The first region lies directly apical to the nucleus and contains well-developed rough and smooth endoplasmic reticulum, together with Golgi bodies. The second region contains electron dense granules, previously described as aggregations (siderosomes) of the iron storage protein ferritin (Nesson & Lowenstam, 1985; Kim et al., 1989) (Fig. 3B). The third region, situated between the second region and the surface of the tooth cusp, is composed of a microvillus border, interspersed with mitochondria, that surrounds the entire cusp surface above the junction zone. There is no difference between the anterior and posterior surfaces, in terms of the relative stage of development of the cells, attached to the major lateral teeth from rows 10 to 18.

Few granules are present within the cusp cells surrounding the nonmineralized tooth rows, 10 to 12, and the microvilli are poorly developed, extending only 1–2 μm into the cell cytoplasm (Fig. 4A–F). However, by row 12 an increasing number of mitochondria were observed near the

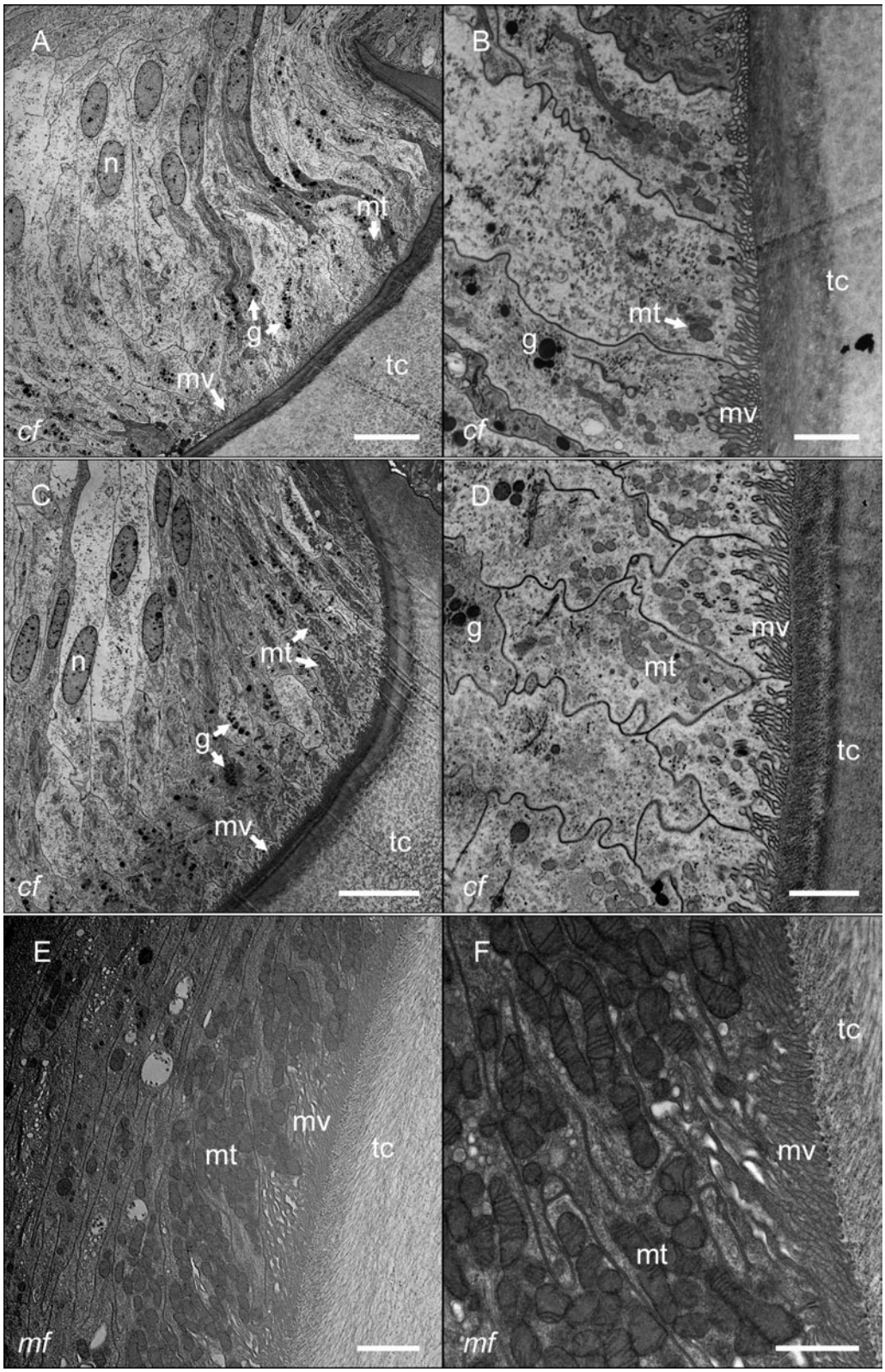

Figure 4. TEM micrographs of cell development within the apical cusp epithelium between the nuclei (n) and tooth cusp (tc) from rows 10 to 12. (**A**,**B**) At tooth row 10, three rows prior to the onset of mineralization in the cusps, only a small number of mitochondria (mt), granules (g) and relatively undeveloped microvilli (mv) are apparent within the tissue. (**C**,**D**) Rows 11 and (**E**,**F**) 12 are similar in appearance to row 10, with the exception of the number of mitochondria, which begin to accumulate around the microvilli, especially toward the cusp tip. Scale bars = (**A**, **C**) 10 μm, (**B**, **D**, **E**) 2 μm, (**F**) 1 μm.

microvilli, particularly toward the cusp tip (Fig. 4E,F). The onset of iron mineralization begins at tooth row 13, one prior to the orange tooth row (see Fig. 3A), as evidenced by the nucleation of mineral in association with the tooth organic matrix (Fig. 5A,B). Significant changes in cusp cell ultrastructure occur at this tooth row, including a dramatic increase in the length and number of microvilli bordering the tooth and a sudden rise in the number of granules within the apical cytoplasm (Fig. 5A,B). By row 14, the tooth cusp takes on its characteristic orange coloration (see Fig. 3A) due to continued mineral deposition within the posterior region of the cusp (Fig. 5C,D). The microvilli continue to develop following the onset of mineralization, extending between 5 and 8 μm from the apical cytoplasm by row 18 (Figs. 5E,F, 6A–F). A large number of granules remain in the apical cytoplasm following the onset of mineralization right up to tooth row 18. Conversely, fewer mitochondria are observed surrounding the microvilli from row 15 compared to the previous (orange) tooth row (Figs. 5E,F, 6A–F). By row 19, the posterior surface of the tooth becomes heavily mineralized with iron, precluding the use of conventional sectioning techniques for TEM in this and subsequent tooth rows.

The EFTEM iron maps reveal individual ~8-nm particles containing iron, distributed throughout the cusp cell cytoplasm from as early as tooth row 7 onward. The size and composition of these particles are consistent with the cores of the iron storage protein ferritin (Mann, 2001). In addition, aggregations of these iron particles were also observed at row 7 (Fig. 7A,B). A considerable degree of variation was observed in both the electron density and structure of granules within the apical cytoplasm (Fig. 8A–D). While the majority of electron dense bodies within the granule region were found to contain iron, it is evident that a number of noniron containing granules were also present (Figs. 8C,D, 9A,B). The major element in the noniron containing granules was discovered to be nitrogen (Fig. 9C), while the iron-rich granules were also found to be rich in nitrogen and oxygen (Fig. 9C,D). EELS spectroscopy confirmed that these were the only detectable elements within the granules. Notably, ~8-nm iron-containing particles, as observed throughout the cytoplasm, were also detected within the microvilli surrounding the tooth cusp (Fig. 10A,B). Similar particles were never observed within the tooth cusp itself.

Discussion

These data clearly show for the first time the intimate linkage between the developmental changes in the cusp cells and the onset of tooth mineralization. In particular, the microvilli, which appear more like simple interdigitating membranes early in cusp development, lengthen substantially during this process. This extension appears to be synchronized with the proliferation of iron-containing siderosomes within the tissues and strongly suggests that, for *A. hirtosa*, tooth row 13 is a pivotal point in the iron mineralization process.

The use of EFTEM revealed that the accumulation of iron-containing granule aggregations in cells surrounding the major lateral tooth cusps first occurs at tooth row 7, a finding that is contrary to earlier studies on *A. hirtosa*, where iron was not observed until immediately prior to the onset of mineralization (Kim et al., 1989). However, it is likely that the Perl's Prussian blue technique used in this earlier study was not sensitive enough to detect iron in these earlier tooth rows. The reason for the presence of iron in the cusp cells prior to its dramatic influx at row 13 is unclear, although the coinciding accumulation of iron at the junction zone (Macey & Brooker, 1996; Shaw et al., 2008*b*) in these tooth rows suggests that some of this iron may pass from the cusp cells to the junction zone and thus prepare the cusp for the onset of mineralization at row 13.

Previous researchers have placed little emphasis on the cusp cells attached to the anterior surface of the major lateral teeth, which undergo the same developmental changes as the cells on the posterior surface, including the accumulation of large numbers of siderosomes. Curiously, the number of granules within the anterior and posterior cusp cells is similar, despite the obvious preferential deposition of iron within the posterior cusp region of the tooth. For iron to pass from the anterior surface, through the tooth core, and on to the posterior surface nucleation sites, the tooth core (apatite) region must not be chemically and/or structurally conducive to iron precipitation. The coordinated influx of iron from both the anterior and posterior cusp epithelium, in addition to delivery from the junction zone (Shaw et al., 2008*b*) would be advantageous for rapidly achieving ion supersaturation at the onset of mineralization, a critical factor required for crystal nucleation and stable growth. At latter stages of the tooth mineralization process, the iron within the anterior cusp epithelium may be utilized for mineralizing the tab region and the thin veneer of lepidocrocite, both of which extend part way down this surface from the cusp tip in this species (Lee et al., 1998; Shaw et al., 2008*b*).

Both EFTEM and EELS have demonstrated that the electron dense aggregations within the apical cusp cells are primarily comprised of varying combinations of iron, nitrogen, and oxygen. An individual granule can also contain a mixture of both discreet iron and noniron components. Notably, both iron and noniron containing granules were found to be nitrogen rich. This nitrogen may be derived from the protein fraction of the iron storage molecule ferritin (Nomura & Isakozawa, 1979). At this stage it is unknown whether the nitrogen in the noniron-containing granules is associated with the empty iron storage protein apoferritin, which may remain in the cytoplasm following the release of the iron core. The oxygen observed in association with the iron-containing granules is likely to be asso-

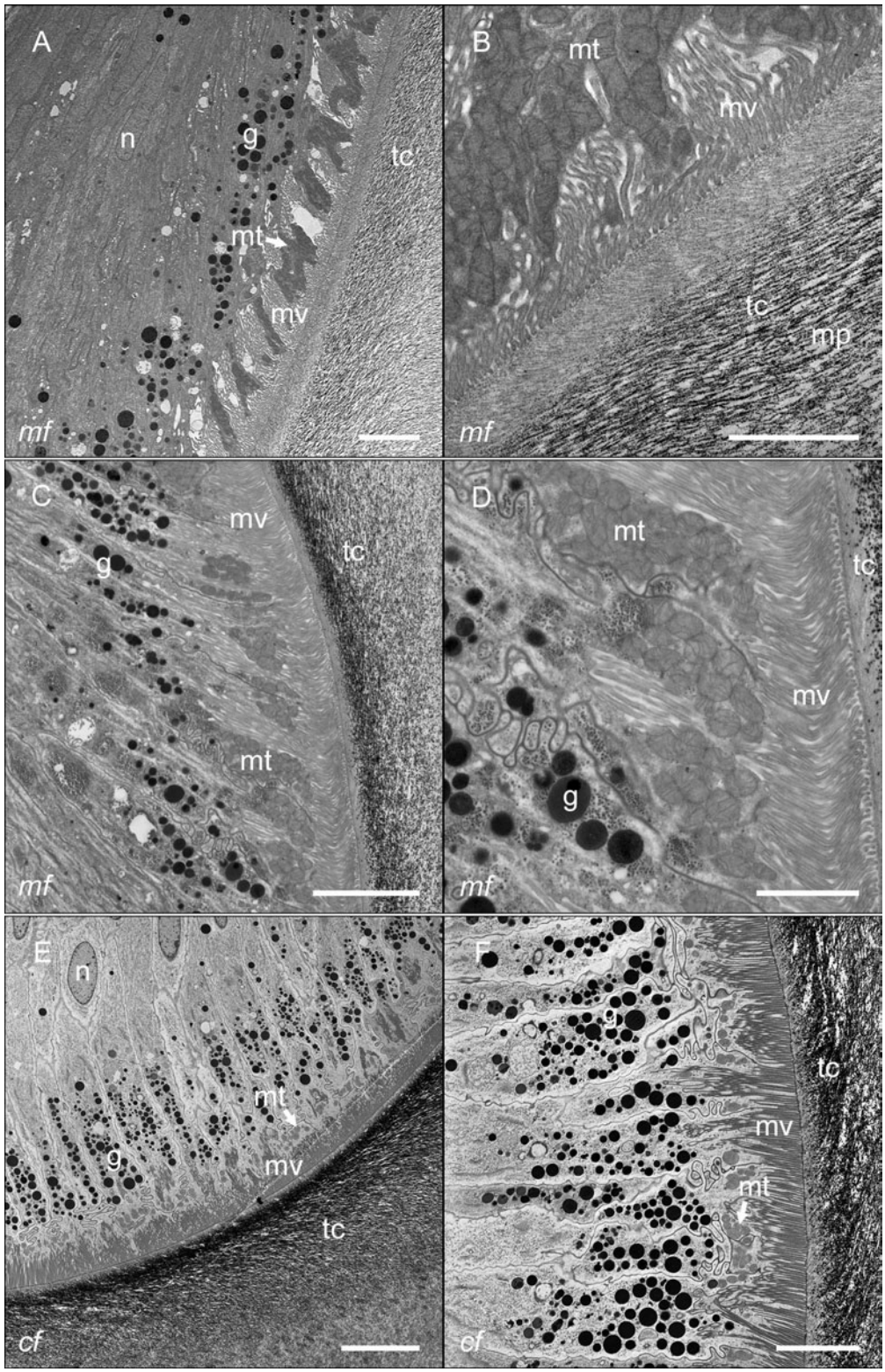

Figure 5. TEM micrographs of cell development within the apical cusp epithelium between the nuclei (n) and tooth cusp (tc) from rows 13 to 15. (**A**,**B**) At the onset of cusp mineralization at tooth row 13, there is a dramatic increase in the number of granules (g) within the apical cytoplasm and the microvilli (mv) increase in length. The first evidence of mineral precipitation (mp) on the tooth organic matrix can also be observed. (**C**,**D**) At rows 14 and (**E**,**F**) 15, granules continue to accumulate in the tissue and the microvilli continue to elongate. There are also fewer mitochondria surrounding the microvilli at row 15 compared to that observed in the previous row. Scale bars = (**E**) 10 μm, (**A**, **C**, **F**) 5 μm, (**B, D**) 2 μm.

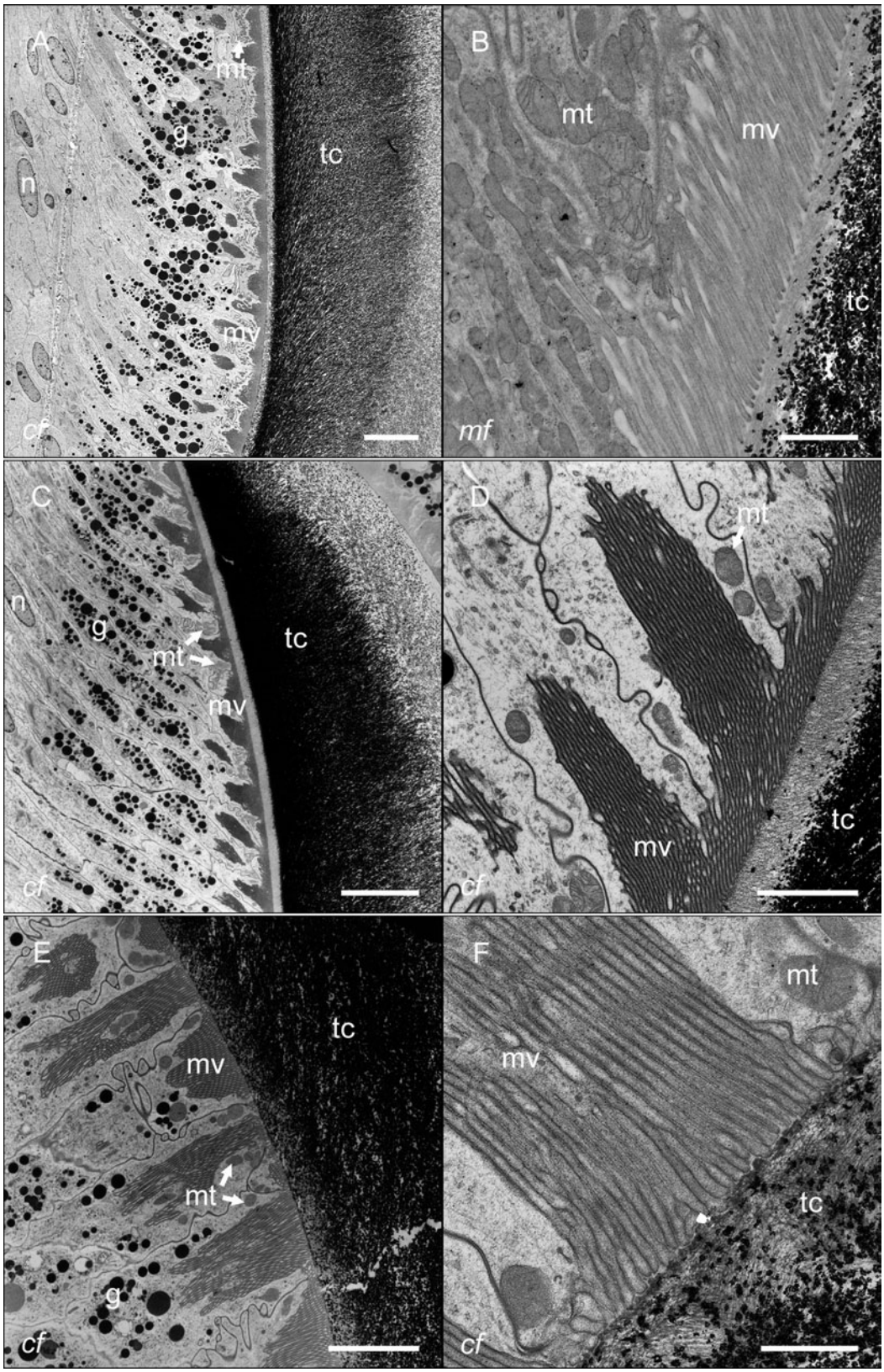

Figure 6. TEM micrographs of cell development within the apical cusp epithelium between the nuclei (n) and tooth cusp (tc) from rows 16 to 18. (**A**,**B**) At tooth rows 16 and (**C**,**D**) 17, increasing amounts of mineral can be observed within the cusps. The microvilli (mv) now extend well into the apical cytoplasm and large aggregations of granules (g) persist in the tissue. (**E**,**F**) Few mitochondria are present around the microvillus bundles by row 18. Scale bars = (**A**, **C**, **E**) 10 μm, (**D**) 2 μm, (**B**, **F**) 1 μm.

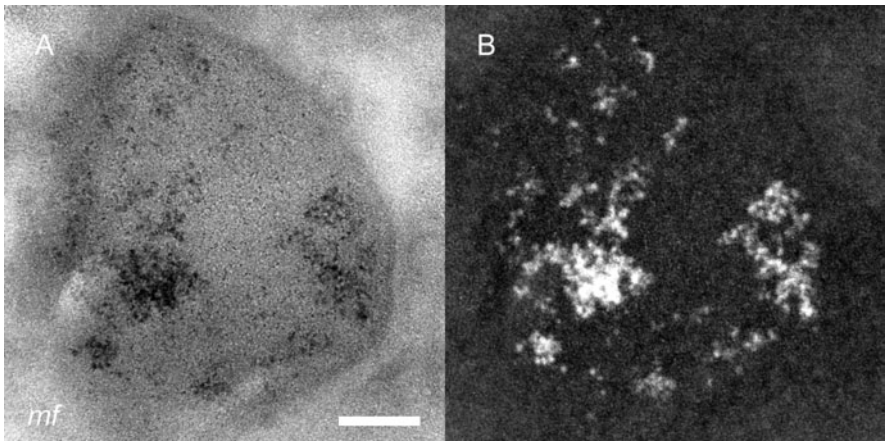

Figure 7. TEM micrograph indicating (**A**) the presence of an electron dense aggregation within the cusp cell epithelium at tooth row 7, which is (**B**) shown to be comprised of iron in the associated EFTEM iron map. Scale bar = 100 nm.

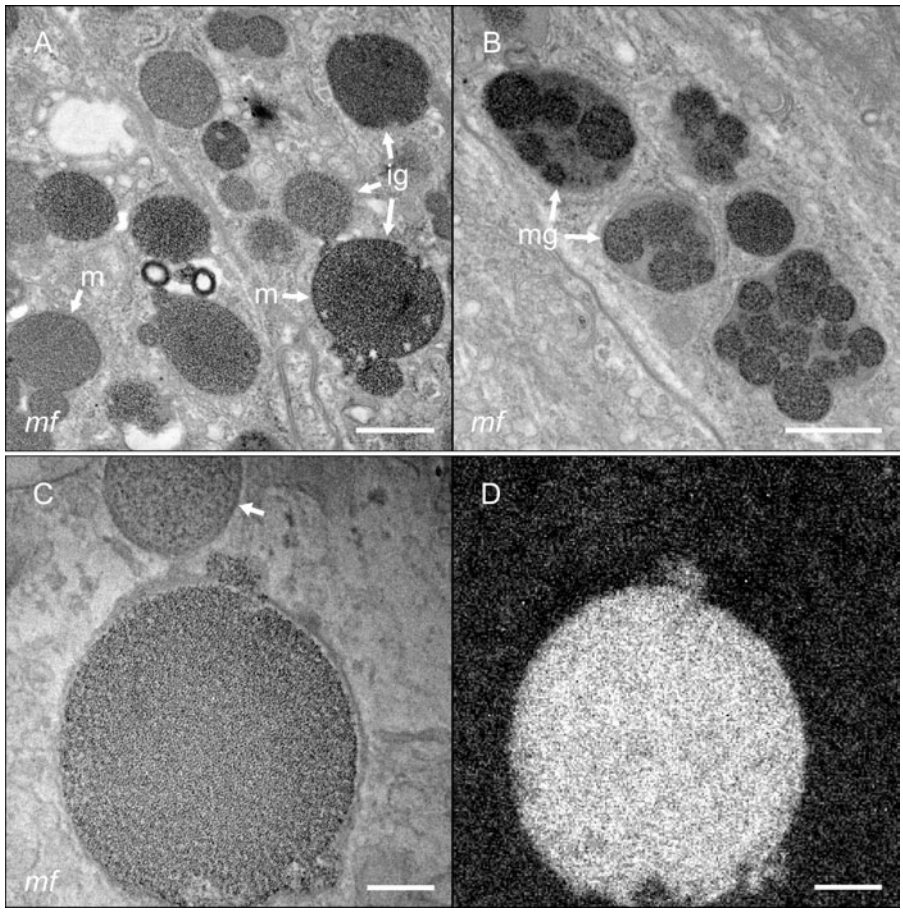

Figure 8. Granule types within the apical cusp cells following the onset of mineralization at tooth row 13. (**A**,**B**) TEM micrographs showing isolated (ig) and multiple granules (mg) of varying electron density, with and without membranes (m). (**C**) The bright field TEM micrograph and respective (**D**) EFTEM elemental map highlight the variability in iron content between granules. Note the absence of iron in the upper granule (arrow) in **C**. Scale bars = (**A**, **B**) 0.5 μm, (**C**, **D**) 200 nm.

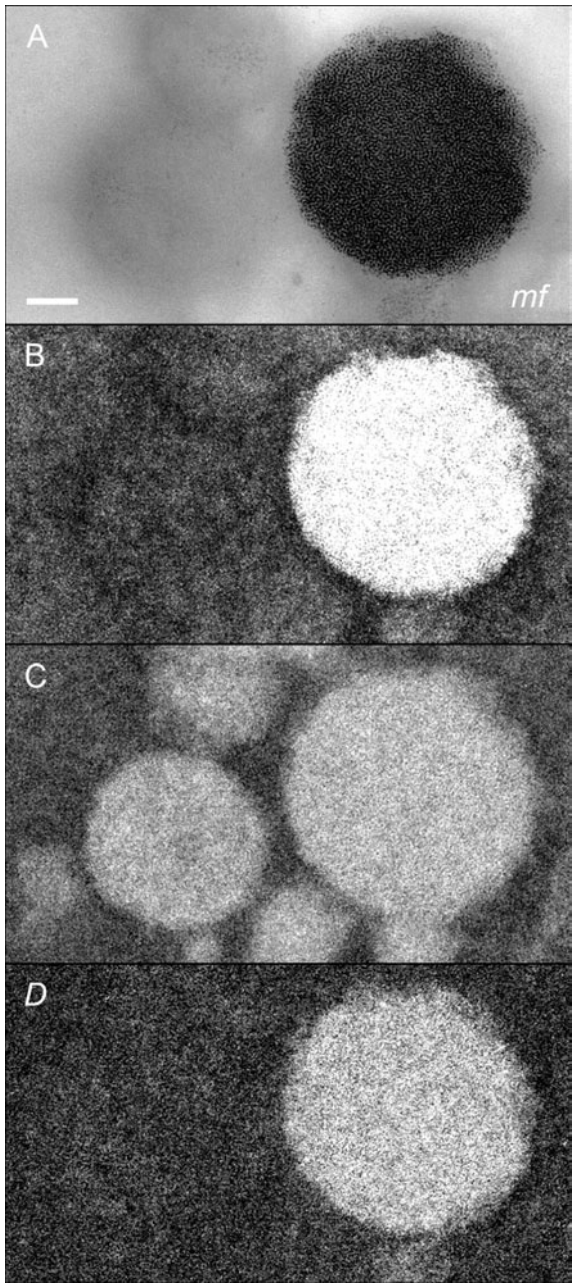

Figure 9. Iron- and noniron-containing granules within the cusp epithelium at tooth row 14. (**A**) Bright-field TEM image with associated (**B**) iron, (**C**) nitrogen, and (**D**) oxygen EFTEM maps showing the distribution of these elements within the various granule types. Scale bar = 200 nm.

ciated with the ferrihydrite ($5Fe_2O_3 \cdot 9H_2O$) iron core of ferritin (Lewin et al., 2005).

A detailed study of granule types in the chiton *Lepidochitona hartwegii* (Nesson & Lowenstam, 1985) also reported similar variation in electron density both between, and within, granules and suggested that the less ordered, amorphous material was composed of ferrihydrite bound to the iron storage protein hemosiderin. While the iron-containing siderosomes within the cusp epithelium may be in the form of either ferritin or hemosiderin, the exact nature and function of the remaining granules require further investigation. Studies, using cryopreparation to prevent the loss of soluble elements, may be valuable for the detection of precursor elements that are required for matrix formation and tooth mineralization.

This article also confirms that analysis of the apical cusp cells using the latest available technology, in this case EFTEM, is critical if a complete picture of events is to be obtained. While earlier researchers observed these electron dense particles within the cytoplasm (Nesson & Lowenstam, 1985; Kim et al., 1989), this study is the first to confirm, *in situ*, the presence of iron, and that these ferritin cores are present within the microvillus bundles. In this regard, microwave-assisted fixation may also have played a role in improving the retention of the ferritin cores compared to conventional fixation methods. The absence of these cores within the extracellular compartment of the tooth cusp suggests that they are solubilized at some point prior to, or immediately following, their passage through the microvillus border. No evidence of exocytosis was observed along the microvilli membranes.

The large number of mitochondria within the apical region of the cell prior to the onset of mineralization suggests that these organelles also play a major role in cusp mineralization. Mitochondria have been suggested as being responsible for providing energy required for the active transport of solubilized iron across the microvilli and into the tooth cusp against a significant concentration gradient (Nesson & Lowenstam, 1985; Kim et al., 1989). Although the mitochondria surrounding the cusp are likely to provide the energy required for the transport of iron into the cusp, their role may not be solely limited to energy production. The role of the mitochondria in cellular respiration, where molecular oxygen is consumed and hydrogen ions are produced (Stryer, 1999), is likely to result in a strongly reductive and acidifying environment near the microvilli. If sustained, these conditions are likely to be mirrored within the extracellular compartment of the tooth cusp, which would assist in maintaining iron in its soluble form until a critical density of ions is reached for precipitation to occur at nucleation sites on the organic matrix. Furthermore, the decline in the number of mitochondria following the onset of mineralization also suggests that the cusp cells no longer need to maintain this reducing environment, which would further promote continued crystal growth.

The continued extension of the microvilli as mineralization progresses may be linked to the decreasing concentration gradient between iron in the cells and in the teeth as increasing amounts of this element are transported into the cusps. The increased surface area provided by the continued elongation of the microvilli would facilitate enhanced ion

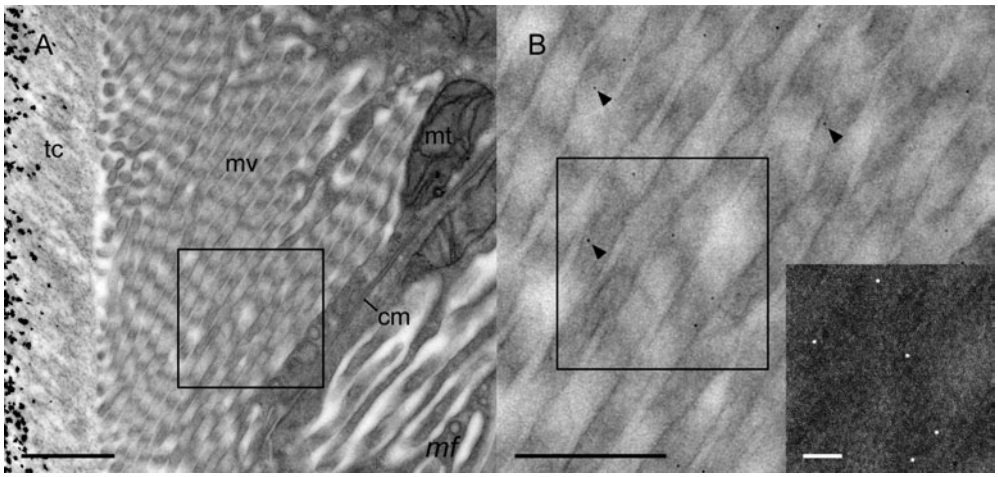

Figure 10. TEM micrographs of the microvilli (mv) bordering the posterior surface of the major lateral tooth cusp (tc) at row 14. **A:** Numerous electron dense particles, characteristic of ferritin, can be seen within the cytoplasm between the microvillus bundles near the cell membrane (cm) and mitochondria (mt). **B:** At higher magnification (square region marked in **A**), these ~8-nm particles (arrowheads) are clearly resolved within the microvilli and are shown to contain iron in the EFTEM iron map (inset). Scale bars = (**A**) 1 μm, (**B**) 500 nm, inset 100 nm.

transport across the apical border (Lange, 2000), permitting greater control over the environment within the extracellular cusp compartment. It is difficult to draw further analogies between the development of the cusp epithelium and epithelia in other biomineralizing systems due to the unique structure of the radula itself, which consists of repeating rows of teeth and tissue, with each row at a different stage of development at any given time.

Crystal nucleation on the posterior cusp face begins at row 13. Notably, the size of these initial crystals varies between individuals and, to some extent, within different regions of the cusp. In *A. hirtosa*, the radula is produced at a rate of ~0.40 tooth rows per day (Shaw et al., 2002, 2008*c*), and as such, there is likely to be some variation in the stage of mineralization between the individuals examined purely as a result of differences in the time of dissection. However, the high level of consistency, with respect to the position of the orange tooth at row 14 (Shaw et al., 2008*b*), supports the idea that cell development, the attainment of ion supersaturation and crystal nucleation, proceed rapidly and with high predictability.

Advances in methods of tissue preservation, such as microwave-assisted fixation and the application of techniques, such as EFTEM and EELS, to the study of biological samples, have provided critical new information for interpreting the cellular mechanisms of tooth mineralization in chitons. Furthermore, this systematic row-by-row investigation of the cusp cell epithelium provides new data on the cellular events leading up to, and following, the onset of tooth mineralization, and complements and expands upon earlier studies of the cusp cell epithelium (Nesson & Lowenstam, 1985; Kim et al., 1989).

Acknowledgments

This research was funded by an Australian Research Council Discovery Grant (DP0559858) to David J. Macey. The authors acknowledge the facilities, scientific and technical assistance of the Australian Microscopy & Microanalysis Research Facility at the Centre for Microscopy, Characterisation & Analysis, The University of Western Australia, a facility funded by The University, State and Commonwealth Governments. Many thanks to Gordon Thomson at Murdoch University for his advice on histological preparations. Preliminary work was also performed in the laboratory of Prof. Brigid Heywood at Keele University, England, United Kingdom.

References

Barbosa, S., Byrne, M. & Kelaher, B. (2008). Bioerosion caused by foraging of the tropical chiton *Acanthopleura gemmata* at One Tree Reef, southern Great Barrier Reef. *Coral Reefs* **27**(3), 635–639.

Brydson, R. (2001). *Electron Energy Loss Spectroscopy*. Emeryville, CA: Telos Springer-Verlag.

Hanaichi, T., Sato, T., Iwamoto, T., Malavasi-Yamashiro, J., Hoshino, M. & Mizuno, N. (1986). A stable lead by modification of Sato's method. *J Electron Microsc (Tokyo)* **35**(3), 304–306.

Kim, K.S., Macey, D.J., Webb, J. & Mann, S. (1989). Iron mineralization in the radula teeth of the chiton *Acanthopleura hirtosa*. *Proc R Soc Lond B Biol Sci* **B237**, 335–346.

Lange, K. (2000). Microvillar ion channels: Cytoskeletal modulation of ion fluxes. *J Theor Biol* **206**(4), 561–584.

Leapman, R.D. (2004). Novel techniques in electron microscopy. *Curr Opin Neurobiol* **14**(5), 591–598.

Leapman, R.D. & Aronova, M.A. (2007). Progress in electron energy loss spectroscopy, elemental mapping and elemental tomography of biological structures. *Microsc Microanal* **13**(Suppl. 2), 460–461.

Lee, A.P., Webb, J., Macey, D.J., van Bronswijk, W., Savarese, A. & De Witt, C. (1998). *In situ* Raman spectroscopic studies of the teeth of the chiton *Acanthopleura hirtosa*. *J Biol Inorg Chem* **3**, 614–619.

Lewin, A., Moore, G.R. & Le Brun, N.E. (2005). Formation of protein-coated iron minerals. *Dalton Trans* **22**, 3597–3610.

Lowenstam, H.A. (1962). Magnetite in denticle capping in recent chitons (Polyplacophora). *Bull Geol Soc Amer* **73**, 435–438.

Macey, D.J. & Brooker, L.R. (1996). The junction zone: Initial site of mineralization in radula teeth of the chiton *Cryptoplax striata* (Mollusca: Polyplacophora). *J Morphol* **230**, 33–42.

Macey, D.J., Brooker, L.R., Webb, J. & St. Pierre, T.G. (1996). Structural organization of the cusps of the radular teeth of the chiton *Plaxiphora albida*. *Acta Zool* **77**(4), 287–294.

Mann, S. (2001). *Biomineralization, Principals and Concepts in Bioinorganic Materials Chemistry*. Oxford: Oxford University Press.

McDonald, K.L., Morphew, M., Verkade, P. & Müller-Reichert, T. (2007). Recent advances in high-pressure freezing. In *Electron Microscopy: Methods and Protocols*, Kuo, J. (Ed.), pp. 143–173. Totowa, NJ: Humana Press Inc.

Nesson, M.H. & Lowenstam, H.A. (1985). Biomineralization processes of the radula teeth of chitons. In *Magnetite Biomineralization and Magnetoreception in Organisms*, Kirshvink, J.L., Jones, D.S. & MacFadden, B.J. (Eds.), pp. 333–361. New York: Plenum Press.

Nomura, S. & Isakozawa, S. (1979). Detection of nitrogen from a ferritin particle by means of energy loss spectroscopy. *J Electron Microsc (Tokyo)* **28**(2), 138–140.

Runham, N.W. (1963). A study of the replacement mechanism of the pulmonate radula. *Q J Microsc Sci* **104**(2), 271–277.

Scheibling, R.E. (1994). Molluscan grazing and macroalgal zonation on a rocky intertidal platform at Perth, Western Australia. *Aust J Ecol* **19**, 141–149.

Shaw, J.A., Brooker, L.R. & Macey, D.J. (2002). Radular tooth turnover in the chiton *Acanthopleura hirtosa* (Blainville, 1825) (Mollusca: Polyplacophora). *Molluscan Res* **22**, 93–99.

Shaw, J.A., Macey, D.J. & Brooker, L.R. (2008*a*). Radula synthesis by three species of iron mineralizing molluscs: Production rate and elemental demand. *J Mar Biol Assoc UK* **88**(03), 597–601.

Shaw, J.A., Macey, D.J., Brooker, L.R., Stockdale, E.J., Saunders, M. & Clode, P.L. (2008*b*). The chiton stylus canal: An element delivery pathway for tooth cusp biomineralization. *J Morphol* (in press). [http://www3.interscience.wiley.com/journal/109771912/issue]

Shaw, J.A., Macey, D.J., Clode, P.L., Brooker, L.R., Webb, R.I., Stockdale, E.J. & Binks, R.M. (2008*c*). Methods of sample preparation of epithelial tissue in chitons (Mollusca: Polyplacophora). *Amer Malacol Bull* **25**, 35–41.

Steneck, R.N. & Watling, L. (1982). Feeding capabilities and limitation of herbivorous molluscs: A functional group approach. *Mar Biol* **68**, 299–319.

Stryer, L. (1999). *Biochemistry*. New York: W.H. Freeman and Company.

Webster, P. (2007). Microwave-assisted processing and embedding for transmission electron microscopy. In *Electron Microscopy Methods and Protocols*, Kuo, J. (Ed.), pp. 47–65. Totowa, NJ: Humana Press.

Weiner, S. (2008). Biomineralization: A structural perspective. *J Struct Biol* **163**(3), 229–234.

Weiner, S. & Addadi, L. (2002). At the cutting edge. *Science* **298**(5592), 375–376.